Journal of Engineering Mathematics, Vol. 12, No. 4, October 1978
Sijthoff & Noordhoff International Publishers–Alphen aan den Rijn
Printed in The Netherlands

The numerical solution of the Navier–Stokes equations for a three-dimensional laminar flow in curved pipes using finite-difference methods

D. F. ROSCOE

Department of Applied Mathematics and Computing Science, University of Sheffield, Sheffield, U.K.

(Received October 21, 1977)

SUMMARY

The numerical method presented treats the primitive-variable form of the Navier–Stokes equations. It is shown how to treat the generalised orthogonal coordinate form of the equations in order to retain the numerical stability of the linearised equations when these are approximated by finite differences. A property analogous to diagonal dominance in more simple systems is shown to exist for the complete set of difference approximations to the flow equations so that the matrix of the finite-difference equations has all of its eigenvalues in the left-hand half-plane. It follows that the linearized equations are unconditionally stable. An entirely new difference scheme for the continuity equation is derived and shown to be superior to the more commonly used "central-difference" approximations for the high-Reynolds-number flow considered. The total "package" is tested against experiment on a shear flow through a 90° rectangular bend. The experimental measurements are of total-pressure distributions, and these indicate the presence of a strong secondary flow. The computed results give a close agreement to the experimental results.

1. Introduction

In [1], Roscoe presented a numerical procedure for the solution of the primitive-variable form of the Navier–Stokes equations for low Reynolds numbers in straight rectangular pipes. The present paper extends this to the case of pipes having boundaries that are constant-coordinate surfaces in arbitrary curvilinear coordinate systems, and for laminar flows having higher Reynolds numbers than those calculable by the earlier method.

The procedure is then tested against experimental data obtained from a "quasi-laminar" flow of air through a curved duct having a rectangular cross section, see Joy [2]. The experimental details are briefly outlined in Section 4. The main feature of the flow is a strong secondary flow which causes the stream surfaces to twist through about 100° as they come through the bend. This particular effect is well predicted by the given procedure.

The data obtained by Joy were originally selected by Hetherington as being a suitable test problem for any method that laid claim to being able to predict the secondary flow components that exist in flows along curved pipes. The same problem was used by Stuart and Hetherington [3], to test the viability of a three-dimensional streamline-curvature procedure developed by them. A complete report is given by Stuart [4]. This procedure was successful to a degree, but it only treated the inviscid problem, and like the methods developed by Spalding and Patankar, [5], it basically considered the flow as parabolic and was therefore unable to cope with flows containing any recirculation. Since the present method treats the fully elliptic equations it does not suffer from this particular drawback,

although there is naturally a penalty paid in terms of computing time and storage requirements.

Stuart reports in [4], that in order to obtain iterative convergence of the streamline-curvature method using Joy's data it was necessary to heavily under-relax successive solutions, and even then there was a tendency for his solutions on the inside of the bend to oscillate slightly. He attributes the failure of the method to deal effectively with the flow in this region to the separation of the boundary layer in the physical flow. A similar unsteady behaviour was manifest in the solutions given in the present paper, the magnitude of the oscillations being of the order 3%. Given Stuart's observation, and that the present procedure performed satisfactorily on artificial data it seems likely that the source of the problem is the failure of an essentially linear-equation-solution algorithm to deal adequately with flow regions where the flow is about to separate, or has separated. In spite of this unsatisfactory situation, it is clear from the presented results that the nature and magnitude of the secondary flow components are well predicted.

2. The Navier–Stokes equations

Define the terms

ν = kinematic viscosity,
ρ = fluid density,
p = static pressure,
y^j = Cartesian coordinates for $j = 1, 2, 3$,
u^j = velocity components in Cartesian coordinate directions for $j = 1, 2, 3$,
x^j = curvilinear coordinates for $j = 1, 2, 3$,
v^j = velocity components in curvilinear coordinate directions for $j = 1, 2, 3$,
g^{ij} = components of the metric tensor, $i, j = 1, 2, 3$,
g = $\det(g^{ij})$,
∇^2 = Laplacian.

With these notations, one form of the Navier–Stokes equations in curvilinear coordinates is given by

$$v^i \frac{\partial}{\partial x^i}\left(\frac{\partial y^t}{\partial x^s} v^s\right) - \frac{\nu}{\sqrt{g}} \frac{\partial}{\partial x^i}\left(\sqrt{g}\, g^{ij} \frac{\partial}{\partial x^j}\left(\frac{\partial y^t}{\partial x^s} v^s\right)\right) = -\frac{1}{\rho} \frac{\partial x^s}{\partial y^t} \frac{\partial p}{\partial x^s}, \quad t = 1, 2, 3, \tag{1}$$

and

$$\frac{\partial}{\partial x^i}(\sqrt{g}\, v^i) = 0. \tag{2}$$

The summation convention is used. Equations (1) are the momentum equations, and equation (2) is the mass-conservation equation for an incompressible fluid. Note that in orthogonal coordinate systems, $g^{ij} = 0$ for $i \neq j$ so that mixed second-order derivatives do not occur.

Finite-difference treatment of the transport and dissipative terms of (1)

Equations (1) are solved not for v^s directly, but for $u^t = v^s\, \partial y^t / \partial x^s$. Thus the left-hand side of

(1) may be written

$$Tu^t = \left\{ v^i \frac{\partial}{\partial x^i} - \frac{\nu}{\sqrt{g}} \frac{\partial}{\partial x^i} \left(\sqrt{g}\, g^{ij} \frac{\partial}{\partial x^j} \right) \right\} u^t$$

$$= \left(v^i \frac{\partial}{\partial x^i} - \nu \nabla^2 \right) u^t, \qquad t = 1, 2, 3, \tag{3}$$

and

$$T = (v^1 + k_1) \frac{\partial}{\partial x^1} - \nu g^{11} \frac{\partial^2}{\partial (x^1)^2}$$

$$+ (v^2 + k_2) \frac{\partial}{\partial x^2} - \nu g^{22} \frac{\partial^2}{\partial (x^2)^2}$$

$$+ (v^3 + k_3) \frac{\partial}{\partial x^3} - \nu g^{33} \frac{\partial^2}{\partial (x^3)^2}. \tag{4}$$

The operator $\partial/\partial x^i \, (\sqrt{g}\, g^{ij}\, \partial/\partial x^j)/\sqrt{g}$ is the Laplacian written in curvilinear coordinates. In (4) use has been made of $g^{ij} = 0$ for $i \neq j$ for arbitrary orthogonal coordinates. k_1, k_2, k_3 are functions of the geometry and the g^{11}, g^{22} and g^{33} are *positive* functions of the geometry. Finite-difference forms of T are then derived using the methods of [1] so that typically if

$$T_1 = A \frac{\partial}{\partial x^1} - B \frac{\partial^2}{(\partial x^1)^2}, \qquad B > 0, \tag{5}$$

then its finite-difference representation, $\hat{T}_1$, is given by

$$\hat{T}_1 = \frac{A}{\Delta x^1 (1 - e_A)} \{ E_1 - (1 + e_A) + e_A E_1^{-1} \},$$

$$e_A = \exp(A\, \Delta x^1 / B), \tag{6}$$

$$E_1 \phi(x^1) = \phi(x^1 + \Delta x^1),$$

where Δx^1 is the increment in x^1.

Because of the form of T, given in (4), these methods guarantee that the difference representation of T, say $\hat{T}$, is diagonally dominant. If the equations (1) were arranged to solve for the curvilinear components v^s, then the operator corresponding to T in (4) would contain additive geometric terms multiplied by quadratic velocity terms. These additional terms would upset the diagonal-dominance property present in T, and could consequently cause numerical problems.

Finite-difference treatment of pressure and continuity terms

The first step is to rearrange the form of (2) into

$$\frac{\partial}{\partial x^i}(\sqrt{g}\,v^i) = \frac{\partial}{\partial x_i}\left(\sqrt{g}\,\frac{\partial x^i}{\partial y^t}\,\frac{\partial y^t}{\partial x^s}\,v^s\right)$$

$$= \frac{\partial}{\partial x^i}\left(\sqrt{g}\,\frac{\partial x^i}{\partial y^t}\,u^t\right) = 0. \tag{7}$$

In a matrix notation, the Navier–Stokes equations in the form given by (3) and (7) become

$$\begin{bmatrix} \rho\sqrt{g}\,T & 0 & 0 & \sqrt{g}\,\dfrac{\partial x^s}{\partial y^1}\,\dfrac{\partial}{\partial x^s} \\ 0 & \rho\sqrt{g}\,T & 0 & \sqrt{g}\,\dfrac{\partial x^s}{\partial y^2}\,\dfrac{\partial}{\partial x^s} \\ 0 & 0 & \rho\sqrt{g}\,T & \sqrt{g}\,\dfrac{\partial x^s}{\partial y^3}\,\dfrac{\partial}{\partial x^s} \\ \dfrac{\partial}{\partial x^s}\left(\sqrt{g}\,\dfrac{\partial x^s}{\partial y^1}\right) & \dfrac{\partial}{\partial x^s}\left(\sqrt{g}\,\dfrac{\partial x^s}{\partial y^2}\right) & \dfrac{\partial}{\partial x^s}\left(\sqrt{g}\,\dfrac{\partial x^s}{\partial y^3}\right) & 0 \end{bmatrix} \begin{bmatrix} u^1 \\ u^2 \\ u^3 \\ p \end{bmatrix} = \begin{bmatrix} 0 \\ 0 \\ 0 \\ 0 \end{bmatrix} \tag{8}$$

The problem is to obtain a difference representation of the bordering matrix of (8) (i.e., of those terms corresponding to the pressure gradients, and the continuity equation). To this end, notice that the element $\sqrt{g}\,\partial x^s/\partial y^1\;\partial/\partial x^s$ of the matrix is the adjoint of $-\partial/\partial x^s(\sqrt{g}\,\partial x^s/\partial y^1)$, i.e. of the diagonally opposite element in the matrix of (8) with its sign changed. This is easily demonstrated by choosing as a scalar product the volume integral over the cube $0 \leq x^s \leq 1$, $s = 1, 2, 3$, and as the function space the set of all once differentiable functions $\psi(x^1, x^2, x^3)$ that are zero on the surfaces of the cube. Thus, if

$$\Delta = \begin{bmatrix} 0 & 0 & 0 & \sqrt{g}\,\dfrac{\partial x^s}{\partial y^1}\,\dfrac{\partial}{\partial x^s} \\ 0 & 0 & 0 & \sqrt{g}\,\dfrac{\partial x^s}{\partial y^2}\,\dfrac{\partial}{\partial x^s} \\ 0 & 0 & 0 & \sqrt{g}\,\dfrac{\partial x^s}{\partial y^3}\,\dfrac{\partial}{\partial x^s} \\ \dfrac{\partial}{\partial x^s}\left(\sqrt{g}\,\dfrac{\partial x^s}{\partial y^1}\right) & \dfrac{\partial}{\partial x^s}\left(\sqrt{g}\,\dfrac{\partial x^s}{\partial y^2}\right) & \dfrac{\partial}{\partial x^s}\left(\sqrt{g}\,\dfrac{\partial x^s}{\partial y^3}\right) & 0 \end{bmatrix}, \tag{9}$$

then the adjoint of the operator Δ is found by transposing the matrix of (9) and replacing each element by its adjoint. By the previous observation about the adjoints of the individual elements of (9), this gives

$$\Delta^* = -\Delta \tag{10}$$

where the asterisk denotes adjoint.

Equation (10) is equivalent to the statement that the eigenvalues of Δ are purely imaginary, and since the eigenvalue spectrum of an operator characterizes that operator in some sense, it is common-sensical to attempt to preserve this character of Δ in its difference representation, $\hat{\Delta}$ say. Thus we deduce that $\hat{\Delta}$ should be skew symmetric. This observation

has important consequences for the difference representation, as a whole, of (8). In [6] it is shown that if the velocity field is homogeneous (v^i, $i = 1, 2, 3$, constant everywhere), then the difference representation of T, $\hat{T}$, can be written as the sum of a negative definite and a skew-symmetric matrix. If a skew-symmetric representation $\hat{\Delta}$ is then used for Δ, this implies that the matrix representation of (8) is then the sum of a negative semi-definite matrix with two skew-symmetric matrices. It is shown in [6] that such a matrix has all of its eigenvalues in the left-hand half complex plane.

Thus, the linearised equations can be regarded as numerically stable. This property is similar to the property of diagonal dominance in more simple systems.

Difference representation of Δ, method (i)

The easiest way to make $\hat{\Delta}$ skew-symmetric is to approximate the operators $\partial/\partial x^s$ in (9) with the central-difference operator $(E_s - E_s^{-1})/h_s$ where for an arbitrary function $\phi(x^s)$, then $E_s\phi(x^s) = \phi(x^s + h_s)$ and h_s is the incremental step in the direction x^s. That this is the case is easily seen by writing down a few of the diagonally opposite terms, bearing in mind that the functions $\sqrt{g}\,\partial x^s/\partial y^1$ are known functions of geometry. This is the procedure adopted in [1] for fully rectangular geometries.

Despite much experiment with boundary conditions on the pressure, the method would not reproduce the observed experimental results. The failure of the method was finally attributed to the form if $\hat{\Delta}$. To describe the alternative treatment of $\hat{\Delta}$, it is easier and sufficient to work in terms of a Cartesian coordinate system. Define

(u, v, w) = velocity components in directions (x, y, z) respectively,

$(\Delta x, \Delta y, \Delta z)$ = incremental steps in directions (x, y, z) respectively,

$(i\Delta x, j\Delta y, k\Delta z) = (i, j, k) = (x, y, z)$,

u_{ijk} = x-component of velocity at a point (i, j, k), with similar definitions for v_{ijk}, w_{ijk} and p_{ijk}.

Difference representation of Δ, method (ii)

A more realistic form for $\hat{\Delta}$ can be deduced from the following argument: suppose that the fluid being investigated is nearly inviscid; then in studying the motion of a fluid "particle" along a streamline between two points A and B, the intuitive best way of approximating the pressure difference driving the particle is $p_B - p_A$. If this pressure difference is resolved from streamline coordinates into Cartesian coordinates, then essentially an "upwind" differencing of pressure gradients results (i.e. forward or backward according to the direction, + or −, of the appropriate velocity components). Suppose that such "upwind" differences are being used for the pressure gradients; then the continuity terms must be differenced to ensure the skew-symmetry of $\hat{\Delta}$. It is easily found that if $u_{ijk} > 0$ for all (i, j, k), so that at any (i, j, k)

$$\frac{\partial p}{\partial x} \simeq \frac{p_{ijk} - p_{i-1\,jk}}{\Delta x}, \tag{11}$$

then the corresponding term in the continuity equation must be differenced like

$$\frac{\partial u}{\partial x} \simeq \frac{u_{i+1\,jk} - u_{ijk}}{\Delta x} \tag{12}$$

with similar results for the other pressure and continuity terms. Thus, *upwind* schemes for the pressure gradients imply *downwind* schemes for the continuity equation.

More precisely, for a general velocity field, defining

$$S_{ijk} = \text{Sign}(u_{ijk}) = \begin{cases} +1 \text{ if } u_{ijk} > 0, \\ 0 \text{ if } u_{ijk} = 0, \\ -1 \text{ if } u_{ijk} < 0, \end{cases} \tag{13}$$

then approximations (11) and (12) become for pressure

$$\frac{\partial p}{\partial x} \simeq \frac{1}{\Delta x}\left(\frac{(1-S_{ijk})}{2} p_{i+1jk} + S_{ijk}p_{ijk} - \frac{(1+S_{ijk})}{2} p_{i-1jk}\right), \tag{14}$$

and for continuity

$$\frac{\partial u}{\partial x} \simeq \frac{1}{\Delta x}\left(\frac{(1+S_{i+1jk})}{2} u_{i+1jk} - S_{ijk}u_{ijk} - \frac{(1-S_{i-1jk})}{2} u_{i-1jk}\right). \tag{15}$$

Equation (14) derives from the physical argument put forward for the pressure gradients, whilst (15) derives from transposing and miltiplying by (-1) the matrix representing (14).

In (9), these schemes imply that $\partial/\partial x^s$ of the pressure gradient is represented by an *upwind* scheme and $\partial/\partial x^s$ in the continuity equation is represented by a *downwind* scheme.

3. Solution procedure

The complete set of difference equations representing (8) can now be written as

$$\begin{pmatrix} \rho\hat{T} & 0 & 0 & H_x \\ 0 & \rho\hat{T} & 0 & H_y \\ 0 & 0 & \rho\hat{T} & H_z \\ -H_x^* & -H_y^* & -H_z^* & 0 \end{pmatrix} \begin{pmatrix} u \\ v \\ w \\ p \end{pmatrix}_{ijk} = \begin{pmatrix} \gamma_1 \\ \gamma_2 \\ \gamma_3 \\ \gamma_4 \end{pmatrix}_{ijk}, \tag{16}$$

$$2 \le i \le I-1,\ 2 \le j \le J-1,\ 2 \le k \le K-1,$$

where γ_{ijk} is the vector of boundary conditions. H_x and $-H_x^*$ are the difference operators representing $\partial/\partial x$ of the pressure gradient and the continuity equation respectively. These difference operators are defined by (14) and (15) respectively. Similar definitions hold for H_y, H_z and $-H_y^*$, $-H_z^*$. $\hat{T}$ is the difference representation of the momentum operator given by (4). Note that the matrix in (16) has all of the symmetry properties, and hence eigenvalue properties, of the matrix in (8), for any orthogonal curvilinear coordinate system. Consider a member of the first equation of (16) at a point i, j, k written for an SOR solution procedure:

$$u_{ijk}^{n+1} = u_{ijk}^{n} - \varepsilon_{ijk}(\rho\hat{T}u_{ijk}^{n} + H_x p_{ijk}^{n+1}) \tag{17}$$

where $\varepsilon_{ijk} = \lambda/t_{ijk}$, where t_{ijk} is the diagonal element of $\rho\hat{T}$, and λ is a constant, typically of order 0.5. Define a vector $\hat{u}_{ijk}$ by

$$\hat{u}_{ijk}^{n+1} = u_{ijk}^{n} - \rho\varepsilon_{ijk}\hat{T}u_{ijk}^{n}. \tag{18}$$

Equations (17) and (18) give

$$u_{ijk}^{n+1} = \hat{u}_{ijk}^{n+1} - \varepsilon_{ijk}H_x p_{ijk}^{n+1}. \tag{19}$$

Similarly define $\hat{v}_{ijk}$ and $\hat{w}_{ijk}$.

From (16) the representation of the continuity equation is

$$-(H_x^* u_{ijk}^{n+1} + H_y^* v_{ijk}^{n+1} + H_z^* w_{ijk}^{n+1}) = \gamma_{4ijk}. \tag{20}$$

Substitution from (19) for u_{ijk}, and similar equations for v_{ijk}, w_{ijk} into (20) yields

$$(H_x^*\varepsilon_{ijk}H_x + H_y^*\varepsilon_{ijk}H_y + H_z^*\varepsilon_{ijk}H_z)p_{ijk}^{n+1} = H_x^*\hat{u}_{ijk}^{n+1} + H_y^*\hat{v}_{ijk}^{n+1} + H_z^*\hat{w}_{ijk}^{n+1} + \gamma_{4ijk}. \tag{21}$$

This is an equation, in terms of p_{ijk}, derived from and equivalent to the continuity equation.

It follows that given $\hat{u}_{ijk}^{n+1}$, $\hat{v}_{ijk}^{n+1}$ and $\hat{w}_{ijk}^{n+1}$, then (21) may be solved directly for p_{ijk}^{n+1}. If u_{ijk}^{n+1}, v_{ijk}^{n+1} and w_{ijk}^{n+1} are then found using (19), etc., then the new velocity field u_{ijk}^{n+1}, v_{ijk}^{n+1} and w_{ijk}^{n+1} satisfies the continuity equation exactly. Thus, in essence, the solution procedure is as follows:

(i) Set u_{ijk}^{0}, v_{ijk}^{0}, w_{ijk}^{0}.

(ii) Calculate $\hat{u}_{ijk}^{1}$, $\hat{v}_{ijk}^{1}$, $\hat{w}_{ijk}^{1}$ from (18) and similar.

(iii) Calculate p_{ijk}^{1} from (21).

(iv) Calculate u_{ijk}^{1}, v_{ijk}^{1}, w_{ijk}^{1} from (19) and similar. The continuity equation is satisfied.

Repeat steps (ii), (iii) and (iv) until convergence, in some sense, is obtained.

For the numerical examples presented, the following convergence criterion was applied: at step (iii) above, an approximate p_{ijk}^{1} is found from (21) by employing an SOR procedure and performing typically 70 iterations. Thus the residuals in (21) will initially be quite large, and since (21) corresponds to the continuity equation, the residuals in this after step (iv) will be correspondingly large. It is found that after several outer iterations, i.e. steps (ii)→(iv), the residuals in the continuity equation progressively diminish.

The solution is considered attained when the maximum absolute residual in the continuity equation is less than some suitably small number. Equation (21) is essentially a fourth-order elliptic difference equation. This can be seen by expanding the term $-H_x^*\varepsilon_{ijk}H_x p_{ijk}$, i.e.

$$\begin{aligned}
&-H_x^*\varepsilon_{ijk}H_x p_{ijk} = A_i p_{i+2jk} + B_i p_{i+1jk} + C_i p_{ijk} + D_i p_{i-1jk} + F_i p_{i-2jk},\\
&A_i = \tfrac{1}{4}\varepsilon_{i+1jk}(1 - S_{i+1jk}^2),\\
&B_i = \tfrac{1}{2}(\varepsilon_{i+1jk}S_{i+1jk}(1 + S_{i+1jk}) - \varepsilon_{ijk}S_{ijk}(1 - S_{ijk})),\\
&C_i = -\tfrac{1}{4}(\varepsilon_{i+1jk}(1 + S_{i+1jk})^2 + 4\varepsilon_{ijk}S_{ijk}^2 + \varepsilon_{i-1jk}(1 - S_{i-1jk})^2),\\
&D_i = \tfrac{1}{2}(\varepsilon_{ijk}S_{ijk}(1 + S_{ijk}) - \varepsilon_{i-1jk}S_{i-1jk}(1 - S_{i-1jk})),\\
&F_i = \tfrac{1}{4}\varepsilon_{i-1jk}(1 - S_{i-1jk}^2).\\
&\text{N.B. } C_i = -(A_i + B_i + D_i + F_i).
\end{aligned} \tag{22}$$

We can add perspective to this "mess" by noting that in the simple case of $\varepsilon_{ijk} = +1$ for all i,

j and k and for $S_{i-1jk} = S_{ijk} = S_{i+1jk} = \pm 1$ then (22) reduces to the standard three-point form of $\partial^2/\partial x^2$. Since (21) is a fourth-order elliptic equation, it requires for its closure two pieces of information on the pressure at every boundary point. It transpires that half of this information comes from an internal consistency condition, and half comes from appealing to the physics of the problem.

Conditions for internal consistency

Consider (21) applied at $i = 2$, i.e. adjacent to the boundary $i = 1$. At this point, (21) contains the term $(-\varepsilon_{1jk}H_x p_{1jk} + \hat{u}_{1jk})$. But by (19) this term equals u_{1jk}, the boundary velocity. Hence there arises the derivative-type consistency condition to be applied on the boundary $i = 1$,

$$-\varepsilon_{1jk}H_x p_{1jk} + \hat{u}_{1jk} = u_{1jk}. \tag{23}$$

A similar consistency condition holds at every other boundary point. The application of these conditions turns out to be equivalent to the cumbersome procedure applied in [1] at equations (24) and (25). Notice that if $S_{ijk} = 0$ for all i, j, k, then the difference schemes just discussed collapse to the central-difference schemes used in [1]. The discussion on the physical conditions applied to pressure is left until Section 5.

The method as so far described has mass-flow problems, i.e. mass is lost at successive computing planes. The next section describes a procedure that ensures that global mass is conserved when the overall solution procedure has converged. Computational results are presented with and without the application of this procedure.

The global conservation of mass

For simplicity the method will be described for a two-dimensional parallel-sided straight channel. It is instructive to see how mass gets "lost" in the finite-difference formulation. In Figure 1, suppose that $u_{ij} > 0$ all (i, j), then for a general v_{ij} the continuity equation at (i, j) is given by

$$\frac{u_{i+1j} - u_{ij}}{\Delta x} + \frac{0.5(1 + S_{ij+1})v_{ij+1} - S_{ij}v_{ij} - 0.5(1 - S_{ij-1})v_{ij-1}}{\Delta y} = 0. \tag{24}$$

This is the downwind representation given at equation (15). Summation of (24) over $2 \le j \le J-1$ yields

$$\frac{1}{\Delta x}\sum_{j=2}^{J-1}(u_{i+1j} - u_{ij}) + \frac{0.5}{\Delta y}\{(1 - S_{iJ-1})v_{iJ-1} - (1 + S_{i2})v_{i2}\} = 0. \tag{25}$$

The terms $\sum_{j=2}^{J-1}(u_{i+1j} - u_{ij})$ can be interpreted as being proportional to the difference in mass flow across planes $i+1$ and i, evaluated using the trapezium rule for integration. Ideally, this term should be zero. From (25) it is clearly a function of the velocities v_{i2} and v_{iJ-1}. Thus, the second term of (25) $\times$ (-1) represents the loss in mass between planes i and $i+1$. Part of this term $-0.5(1 - S_{iJ-1})v_{iJ-1}$ can be physically interpreted as proportional to that mass of fluid that crosses the line **AB** in Fig. 1(ii). This fluid crosses the plane $i+1$

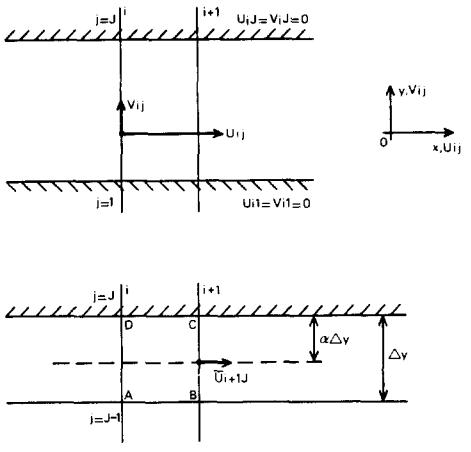

Figure 1. (i) This depicts a parallel channel, boundaries shown shaded, with a flow predominantly in the x-direction.
(ii) This depicts a region near one wall of the channel, and the dotted line parallel to the boundary indicates the line along which the additional velocities $\bar{u}_{iJ}$ are calculated. The velocity $\bar{u}_{i+1J}$ in the diagram is calculated to "pick up" the mass that has escaped across AB.

between BC, but between B and C, there is no provision, numerically, for picking this fluid up again and so it is lost to the calculation. A similar thing occurs at the opposite wall near $j = 2$.

The way this problem has been dealt with in the past is by the use of staggered grids, e.g. [4], [7]. In these systems the computational mesh extends beyond the physical boundaries of the problem to define so-called "fictitious boundaries". Boundary values for velocities on these "fictitious boundaries" are then adjusted to guarantee mass conservation. In three dimensions, staggered meshes are very complicated computationally, and so the author has chosen, at least for the initial development of the present method, to use a single-mesh system. In an attempt to cure the mass-flow problem on the simple mesh, the author proceeded as follows:

(i) between computation lines $j = J - 1$ and J introduce a further computational line (shown dotted in Fig. 1(ii)) distance $\alpha \Delta y$ from $i = J$, $0 < \alpha < 1$. At the point where this dotted line cuts the plane $i + 1$, introduce the velocity $\bar{u}_{i+1J}$, and calculate its magnitude in order to pick up the mass that flowed across AB.

(ii) Introduce this new information into the calculation by using $\bar{u}_{i+1J}$ in the expression for $\partial u/\partial y$ at $(i + 1, J - 1)$ instead of u_{i+1J} as previously.

Repeat the process between $j = 1$ and 2. Apart from acting to reduce mass loss as it is designed to do, the procedure automatically gives a much better treatment of the important term $\partial u/\partial y$ adjacent to solid boundaries. This can be seen in Fig. 2. Figure 2(i) shows a typical u-profile near a solid boundary for a shear flow. Fig. 2(ii) shows the approximation to this profile using the introduced velocity $\bar{u}_{i+11}$. Fig. 2(iii) shows the approximation without the additional velocity. The shaded areas under the curves are proportional to the mass flows across the plane between $0 \leq y \leq \Delta y$.

The calculations of $\bar{u}_{i+11}$ and $\bar{u}_{i+1J}$ are done as follows: with the introduced velocities $\bar{u}_{i+11}$ and $\bar{u}_{i+1J}$, the trapezium rule for the mass flow across plane $i + 1$, M_{i+1} say, gives

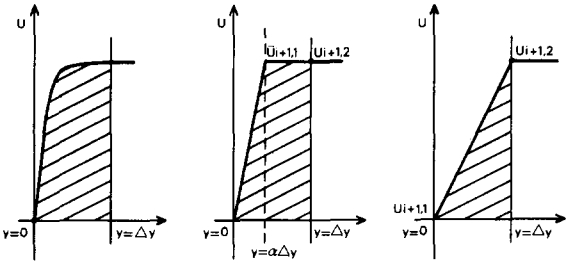

Figure 2. These diagrams are intended only as graphical illustrations of the flow process near a no-slip boundary. They are not drawn from calculations.
(i) This shows a typical velocity profile of velocities, normal to the plane of the diagram, measured at points away from the no-slip boundary at $y = 0$.
(ii) This shows a typical numerical approximation of the profile shown in 7(i), calculated using the mass-flow-conservation procedure described.
(iii) This shows the same profile calculated without the additional velocities $\bar{u}_{i1}$.
In each diagram, the mass flow between $y = 0$ and $y = \Delta y$ is proportional to the shaded area. Thus, it is clear how mass gets lost near boundaries with finite-difference procedures.

$$M_{i+1} = \frac{\Delta y}{2}(\bar{u}_{i+11} - \alpha u_{i+12}) + \Delta y \sum_{j=2}^{J-1} u_{i+1J} + \frac{\Delta y}{2}(\bar{u}_{i+1J} - \alpha u_{i+1J-1}). \tag{26}$$

Since $M_{i+1} - M_i = 0$, then use of (26) and comparison with (25) gives

$$\begin{aligned} \bar{u}_{i+11} - \bar{u}_{i1} - \alpha(u_{i+12} - u_{i2}) &= -\frac{\Delta x}{\Delta y}(1 + S_{i2})v_{i2}, \\ \bar{u}_{i+1J} - \bar{u}_{iJ} - \alpha(u_{i+1J-1} - u_{iJ-1}) &= \frac{\Delta x}{\Delta y}(1 - S_{iJ-1})v_{iJ-1}. \end{aligned} \tag{27}$$

Assuming that $\bar{u}_{i1}$ and $\bar{u}_{iJ}$ are known, equations (27) give $\bar{u}_{i+1J}$ and $\bar{u}_{i+11}$. Knowledge of $\bar{u}_{i1}$ and $\bar{u}_{iJ}$ may be assumed since for $i = 1$, $\bar{u}_{1J}$ and $\bar{u}_{11}$ can be interpolated from the initial data. Values for all i then follow.

This procedure was performed for various values of $\alpha \leq 0.5$. The best value of α appeared to be around $\alpha = 0.2$. The main effect of varying α seemed to be that of moving the positions of the total-pressure contours *near* the walls. For values of α much less than 0.1, the flow near the boundaries became obviously distorted. The probable reason for this occurrence can be seen by considering the first equation of (27) in the limiting case of $\alpha = 0$. In this case $\bar{u}_{i+11}$ and $\bar{u}_{i1}$ are boundary velocities, and are therefore zero by the no-slip boundary condition. However, by (27), their difference is non-zero if $v_{i2} > 0$, and since $v_{i2} > 0$ is perfectly reasonable there is a singular situation. Presumably, for non-zero but decreasing values of α, the equations tend to become singular, resulting in distorted flows near the boundaries.

A possible, but untried, way out of this singular situation may be to set $\alpha = 0$, and to replace the no-slip condition on u_{i1} $(= \bar{u}_{i1})$ and u_{iJ} $(= \bar{u}_{i1})$ by the condition that u_{i1} and u_{iJ} are such that no mass is lost through the boundaries. One would expect such a procedure to be reasonable on coarse computing meshes.

In three-dimensional curvilinear coordinates it is necessary to also have values of the other two velocity components at points where $\bar{u}_{i1}$ and $\bar{u}_{iJ}$ are calculated. In the present circumstances $\bar{u}_{i1}$ and $\bar{u}_{iJ}$ are the main components of the flow velocity, and so the two minor components were extrapolated from the main flow calculations.

4. The experimental problem

The experimental results against which the present method was tested, were obtained by Joy [2]. The duct used by Joy is illustrated in Fig. 3. His measurements were obtained between the planes XX' and YY', the flow being a shear flow of air at approximately 15°C. The mean velocity across the inlet was approximately 65 ft/sec.

A Reynolds number of this flow is about 10^5, and so it is reasonable to assume that this flow is turbulent. However, in the case of very high Reynolds numbers (such as we have in this case), and away from regions of high shear stress, it is possible to ignore the turbulent shear stresses and to treat the flow as effectively laminar in character. It is evident from the experimental results presented here (Figures 5a, 6a and 7a) that away from the walls there are no regions of high shear stress and we can with reasonable confidence assume that the flow can be characterized with a laminar model. This has already been done in a theoretical analysis by Hawthorne [8], and in a numerical analysis by Stuart and Hetherington [3].

The normal-velocity contours at the entrance plane, are given in Fig. 4, and the experimental results at 30°, 60° and 90° round the bend are given in Figs. 5a, 6a and 7a. Note that in these latter figures the symmetry of the flow about the line BB' on the inset of Fig. 3, has been used.

The main feature of the experimental results is a strong secondary flow across the bend. This secondary flow manifests its presence by the anti-clockwise twisting of the total-

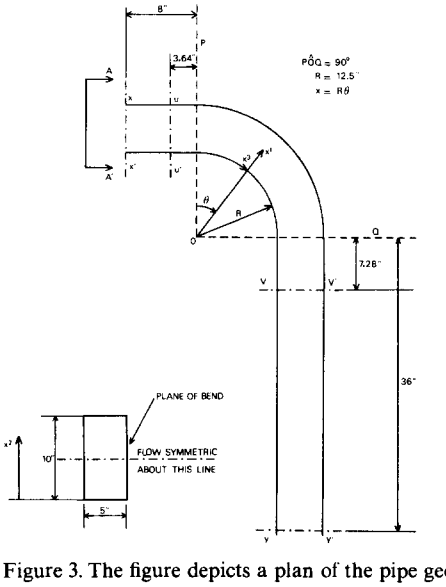

Figure 3. The figure depicts a plan of the pipe geometry, drawn to scale. The physical experiment was performed between planes XX' and YY'. The numerical calculations were performed between UU' and VV'.

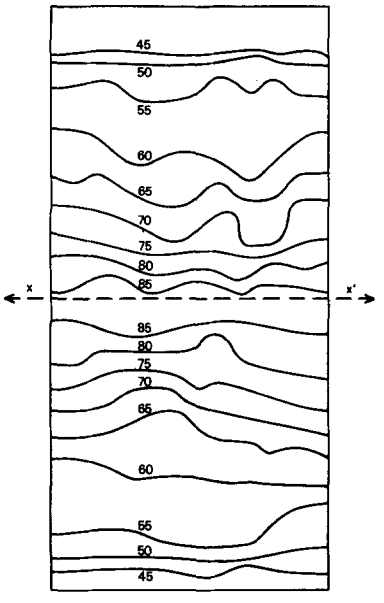

Figure 4. These are the normal-velocity contours measured by Joy on the plane XX'. These contours were used as boundary conditions on the computing plane UU'.

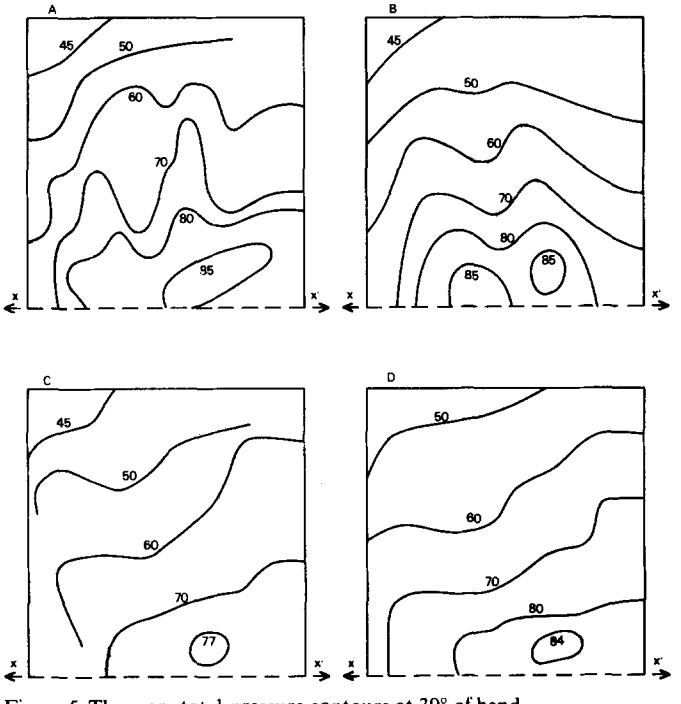

Figure 5. These are total-pressure contours at 30° of bend.

(a) experimental contours

(b) contours calculated using central differences

(c) contours calculated using upwind-downwind differences

(d) contours calculated using upwind-downwind differences with mass-conservation procedure implemented.

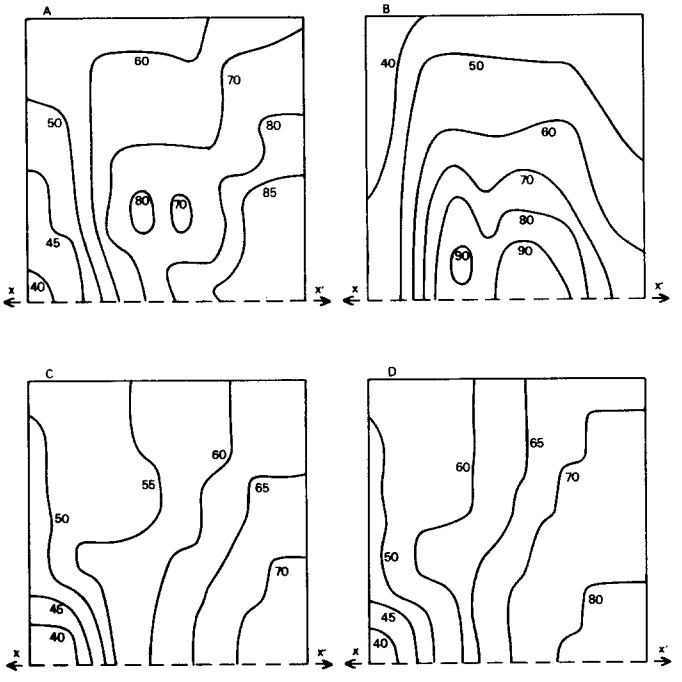

Figure 6. These are total-pressure contours at 60° of bend.
(a) experimental contours
(b) contours calculated using central differences
(c) contours calculated using upwind-downwind differences
(d) contours calculated using upwind-downwind differences with mass-conservation procedure implemented.

pressure surfaces as they progress through the bend. After 90° of bend, these surfaces have turned by about 100°.

Unfortunately, the results of Joy are incomplete in that on the inlet plane he did not specify the tangential (in-plane) velocity field, so that for numerical calculations one is forced to guess the inlet tangential flow field. Both the present author and Stuart and Hetherington [3] assumed that the flow was parallel over the inlet plane. This lack of information caused problems in the present method as explained in Section 6.

5. The numerical problem

The geometry is given in Fig. 3. The computation was done between the planes UU' and VV', mainly to reduce the storage requirements and computation time. On the straight sections, a Cartesian coordinate frame (y^1, y^2, y^3) was employed, whilst on the curved sections the curvilinear system (x^1, x^2, x^3) defined in Fig. 3, was employed.

The coordinate relationships are defined by

$$(y^1, y^2, y^3) = \left\{x^1 \cos\left(\frac{x^3}{R}\right), x^2, x^1 \sin\left(\frac{x^3}{R}\right)\right\} \tag{28}$$

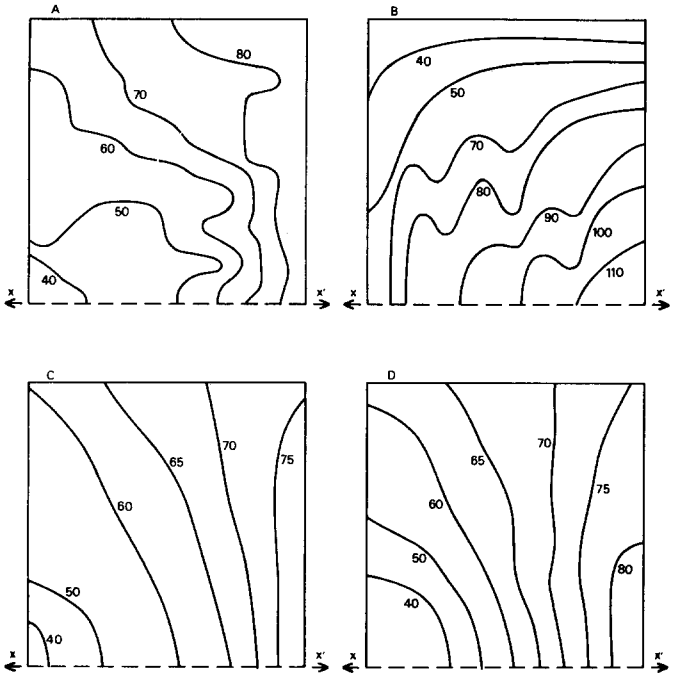

Figure 7. These are total pressure contours at 90° of bend.
(a) experimental contours.
(b) contours calculated using central differences
(c) contours calculated using upwind-downwind differences
(d) contours calculated using upwind-downwind differences with mass-conservation procedure implemented.

giving

$$g^{11} = g_{11} = 1,\ g^{22} = g_{22} = 1,\ g^{33} = g_{33}^{-1} = \left(\frac{R}{x^1}\right)^2, \tag{29}$$

$$g^{ij} = g_{ij} = 0,\ i \neq j, \quad g = |g_{ij}| = \left(\frac{x^1}{R}\right)^2.$$

For an explanation of the general relationships, see for example [8]. The quantities $\partial y^t/\partial x^s$ and $\partial x^s/\partial y^t$ for $s, t = 1, 2, 3$, are given in

$$\left(\frac{\partial y^t}{\partial x^s}\right) = (m^{ts}) = \begin{bmatrix} \cos\left(\frac{x^3}{R}\right) & 0 & -\frac{x^1}{R}\sin\left(\frac{x^3}{R}\right) \\ 0 & 1 & 0 \\ \sin\left(\frac{x^3}{R}\right) & 0 & \frac{x^1}{R}\cos\left(\frac{x^3}{R}\right) \end{bmatrix} \tag{30}$$

and

$$\left(\frac{\partial x^s}{\partial y^t}\right) = (n^{st}) = \begin{bmatrix} \cos\left(\frac{x^3}{R}\right) & 0 & \sin\left(\frac{x^3}{R}\right) \\ 0 & 1 & 0 \\ -\frac{R}{x^1}\sin\left(\frac{x^3}{R}\right) & 0 & \frac{R}{x^1}\cos\left(\frac{x^3}{R}\right) \end{bmatrix} \tag{31}$$

where m^{ts} is the element in *row* t and *column* s and n^{st} is the element in *row* s and *column* t.

Using the operator T defined by (4) and the above relationships, equations (1) become

$$\begin{aligned} &\rho T u^1 + \cos\left(\frac{x^3}{R}\right)\frac{\partial p}{\partial x^1} - \frac{R}{x^1}\sin\left(\frac{x^3}{R}\right)\frac{\partial p}{\partial x^3} = 0, \\ &\rho T u^2 + \frac{\partial p}{\partial x^2} = 0, \\ &\rho T u^3 + \sin\left(\frac{x^3}{R}\right)\frac{\partial p}{\partial x^1} + \frac{R}{x^1}\cos\left(\frac{x^3}{R}\right)\frac{\partial p}{\partial x^1} = 0, \end{aligned} \tag{32}$$

where

$$\begin{aligned} T = {} & v^1\frac{\partial}{\partial x^1} + v^2\frac{\partial}{\partial x^2} + v^3\frac{\partial}{\partial x^3} \\ & - \frac{R}{x^1}\nu\left(\frac{\partial}{\partial x^1}\left(\frac{x^1}{R}\frac{\partial}{\partial x^1}\right) + \frac{\partial}{\partial x^2}\left(\frac{x^1}{R}\frac{\partial}{\partial x^2}\right) + \frac{\partial}{\partial x^3}\left(\frac{R}{x^1}\frac{\partial}{\partial x^3}\right)\right). \end{aligned} \tag{33}$$

The continuity equation (7) becomes

$$\begin{aligned} &\frac{\partial}{\partial x^1}\left(\frac{x^1}{R}\left(\cos\left(\frac{x^3}{R}\right)u^1 + \sin\left(\frac{x^3}{R}\right)u^3\right)\right) + \frac{\partial}{\partial x^2}\left(\frac{x^1}{R}u^2\right) \\ &\quad + \frac{\partial}{\partial x^3}\left(-\sin\left(\frac{x^3}{R}\right)u^1 + \cos\left(\frac{x^3}{R}\right)u^3\right) = 0. \end{aligned} \tag{34}$$

Equations (32) and (34) with T defined by (33) are the curved-section equations for (u^1, u^2, u^3, p).

T is represented by difference schemes discussed in [1], and the pressure and continuity derivatives are represented using the schemes discussed above.

6. Boundary conditions

(i) *Velocities*

The computational inlet plane was taken as UU' in Fig. 3. Normal-velocity profiles were specified on this plane, and were taken as Joy's profiles given in Fig. 4. This procedure was

thought reasonable because numerical experiment showed that the profiles changed very little along straight sections of duct for the types of profiles considered. The in-plane velocity components on UU' were taken as zero.

On the exit plane, the normal derivatives of all three velocity components were taken as zero.

(ii) *Pressures*

We are concerned here with the *physical* boundary conditions on pressure to be used in (21) and not the consistency conditions discussed in Section 3.

On the solid boundaries, for consistency, the static pressures were assumed to be zero. This assumption derives from the inviscid assumption that since the solid boundaries are stream surfaces, then the total pressure is zero upon them. The no-slip condition then implies that the static pressure is zero at the walls. Such an assumption is only possible in the case of high (local and global) Reynolds numbers, and in the present circumstances seems to have been reasonable. Ready support of this approximation may be found in [8], where Hawthorne reporting Joys results remarks (p. 385) that the static pressure variation is very small throughout the flow.

On the exit plane, the normal component of the momentum equation was used to define the normal pressure gradient there.

The inlet plane pressure has yet to be determined. To this end use may be made of the fact that so far the continuity equation has not been solved on the inlet plane. When $\nabla \cdot \boldsymbol{q}$ ($\boldsymbol{q}$ is the velocity vector) is *downwind* differenced we may use it on the initial plane to solve for the normal velocities on the first internal computing plane, hereafter called plane 2.

This leaves the normal momentum equation on plane 2 to be satisfied, and this may be done by using it to prescribe the pressure gradient (*upwind* differenced) over the inlet plane and plane 2. This procedure, whilst perfectly sound in principle relies on a complete knowledge of the inlet-plane velocity field. As previously stated the tangential velocity field was not measured by Joy, and so was assumed for the present calculations to be zero. In practice, satisfying $\nabla \cdot \boldsymbol{q} = 0$ on the inlet plane forced this assumed tangential velocity field strongly onto the flow with the consequence that the resulting solution differed drastically from the experimental results. The main effect was a reduction in the degree of secondary flow compared with the experiment.

The problem of incomplete data on the initial plane was sidestepped by dropping the requirement that $\nabla \cdot \boldsymbol{q} = 0$ be satisfied on the inlet plane, and substituting the condition of zero static pressure over this plane. This assumption was also made by Jǫy [2]. Adopting this procedure does not mean that it is unnecessary to know the inlet-plane tangential velocity field, since values in this velocity field are required in the derivatives normal to plane 2 that are contained in the momentum equations that are tangential to plane 2. All that has happened is that the assumed velocity field is forced much less strongly onto the flow. The major effect of not satisfying $\nabla \cdot \boldsymbol{q} = 0$ at the inlet was a 12% mass loss between the inlet plane and plane 2. It is to be stressed that this mass loss is *not* intrinsic to the method.

7. Aims of the present computation

The main feature of the flow is the presence of the strong secondary flow across the bend. Such secondary flows can have great significance in engineering situation, since they have

associated with them a loss of work capacity in the flow. The reason is that secondary flows can redistribute a large proportion of the total energy of the complete flow system, so that the redistributed flow energy is not always recoverable in terms of mechanical work. Thus, for instance, in a turbine secondary-flow losses can result in the turbine operating significantly below its designed work rate. Thus, the main aim of the present calculation is to predict the presence and magnitude of secondary flows. To this extent, it will be seen that the present calculations have been successful.

8. Computing details

The mesh size used was $8 \times 8 \times 16$ in the (x^1, x^2, x^3) directions respectively. The observed symmetry of profiles on the inlet plane was not used, so that the computation mesh was needlessly coarse in the x^2-direction.

The starting solution was taken as the inlet profile normal to every internal computing plane. Thus, prior knowledge of the secondary flow was *not* introduced into the computation.

Successive solutions moved rapidly from the starting solution into the region of the presented "solutions", and thereafter oscillated, with progressively smaller oscillations. Eventually, oscillations in successive solutions stabilised at about $\pm 3\%$ of the mean solutions.

The machine used was a CDC 7600. After about 50 seconds solutions were within about 10% of those presented with the secondary flow fully predicted. A further 500 seconds were required to bring the solutions to those presented.

9. Results

These are given in Figures 5, 6 and 7. The plotted contours are of

$$(2 \times \text{Total Pressure})^{\frac{1}{2}} = \left(\frac{2p}{\rho} + \boldsymbol{q} \cdot \boldsymbol{q}\right)^{\frac{1}{2}} \tag{35}$$

where $|\boldsymbol{q}|$ is the total velocity, i.e. the contours have dimensions of ft/sec, but they are essentially total-pressure contours. Note that on the entrance plane, $p = 0$ so that the contours there *are* velocity contours.

All figures are drawn looking *upstream* so that the left-hand sides correspond to the *inside* of the bend, and the right-hand sides correspond to the outside of the bend.

These results are presented in terms of these contours, mainly to facilitate the comparison with the experimentally calculated contours, which are given in the same terms. However, it is to be noted that for an inviscid fluid, these contours will coincide with the stream-surface contours, and since the present flow is "almost" inviscid out of the wall region it is reasonable to assume for reasons of continuity that the presented contours are good approximations to the stream-surface contours. Hence, deductions regarding the degree of secondary flow can reasonably be made from the presented results.

Figures 5a, 6a, 7a.
These give the experimentally measured contours at 30°, 60° and 90° respectively.

Figures 5b, 6b, 7b.
These give the computed contours at 30°, 60° and 90° using central-difference representations of the pressure gradients and continuity terms.

Figures 5c, 6c, 7c.
These give the computed contours at 30°, 60° and 90° using upwind/downwind representations of pressure gradients and continuity terms respectively, *without* the method of global mass conservation being applied.

Figures 5d, 6d, 7d.
These give the computed contours at 30°, 60° and 90° using upwind/downwind representations of pressure gradients and continuity terms respectively, but *with* the method of global mass conservation being applied.

Experimental results in Figures 5a, 6a, 7a.
The experimental contours indicate the presence of a strong secondary flow, depicted by the progressive twisting of the total-pressure surfaces as the flow proceeds through the bend. By 90° of bend these surfaces have rotated through approximately 100°. Observe that the region of low energy in the top left of the 30° experimental figure has moved to the bottom left of the experimental figure at 60°. Thus, the flow tends to "back" up against the outside of the bend.

Central-difference results in Figs. 5b, 6b, 7b.
These are the results obtained when the pressure gradients and continuity terms are centrally differenced. These results are very poor. For example, comparison of the 90° numerical results (fig. 7b) with the 30° experimental results (fig. 5a) reveals a certain similarity. This probably indicates that secondary flow is present in these calculations, but in a very weak form. Various experimentation was done with the pressure boundary conditions, but the best results were obtained using those outlined in the section on boundary conditions.

Upwind-Downwind results in Figs. 5c, 6c, 7c.
These are the results obtained without attempting to conserve global mass. The introduction of the upwind-downwind methods for pressure gradients and continuity terms produced a dramatic improvement in the results. The three figures predict quite well the degree of turning in the contours at 30°, 60° and 90° of bend. Unfortunately, although the low-value contours are well predicted, the high-value contours are not. This is due to numerical losses of mass and energy manifesting themselves as losses in the high-energy regions of the numerical flow. It was found that between the second computing plane and the exit plane, there was a mass loss of about 5%, whilst between the first and second computing planes, there was a mass loss of about 12%. This latter, and larger loss was due to the fact that the continuity equation was not solved on the inlet plane causing a large "once and for all" mass loss. The smaller loss was due to the factors described in the section on global mass conservation.

Upwind-Downwind results in Figs. 5d, 6d, 7d.
These computations are similar to those of the previous section; but additional velocities were introduced near the solid boundaries in an attempt to conserve mass flow.

The three figures at 30°, 60° and 90° degrees of bend accurately predict the experimental results and like the previous results give reasonable predictions for the low value contours. Unlike the previous results there have been no significant numerical losses on the high-value contours, and exception the 90° degree results, these high-value contours have also been reasonably well predicted.

The relative poorness of the 90° results is possibly due to the short length of the straight settling section compared to the length of the settling section used experimentally.

It is apparent from the contour plots that there have been no significant numerical losses of energy, and so the technique primarily designed to cut numerical mass loss has been very effective in cutting energy losses. The failure of the solution procedure to obtain a completely converged solution resulted in a mass loss, for the following reason. The downwind difference schemes for the continuity equation effectively make the divergence operator $(\nabla\cdot)$ dependent on the velocity field though the sign (velocity) function (see equation 15). The conservation method derived between equations (24) and (27) implicitly assumes that the numerical equivalent of

$$\nabla^{(n+1)}\cdot \boldsymbol{q}^{(n+1)} = 0 \tag{36}$$

is solved ($\boldsymbol{q}$ denotes velocity field, and superfix $(n+1)$ denotes the $(n+1)$th iterative). In fact, the solution procedure described earlier causes the numerical equivalent of

$$\nabla^{(n)}\cdot \boldsymbol{q}^{(n+1)} = 0 \tag{37}$$

to be solved. Thus, the global-mass-conservation method actually uses the equation

$$\nabla^{(n+1)}\cdot \boldsymbol{q}^{(n+1)} = \varepsilon^{(n+1)} \tag{38}$$

where $\varepsilon^{(n+1)}$ is a field of small residuals, to "conserve" global mass flow. Naturally, since $\varepsilon^{(n+1)} \neq 0$ global mass was not conserved in mid calculation, although for a converged solution, then mass would be conserved. The fact of $\varepsilon^{(n+1)} \neq 0$ caused a systematic mass loss of the order 5% between the second and last computing planes. Unlike the situation in the previous case where mass was lost near the walls, the present procedure seemed to cause the mass to be lost more evenly throughout the flow.

10. Future development

There are problems still remaining within the presented method.

(i) The solution procedure is inadequate for the flow considered, in that the solutions tended to "flutter" by about $\pm 3\%$. A similar phenomenon was reported by Stuart [5] for the same problem, but his calculation was parabolic and he was thus able to contain the instability to the region in which it occurred close to the inside bend of the flow. Stuart attributed the problem to a separation of the boundary layer in the real flow. The failure of the presented method to fully converge also resulted in a mass loss of the order 5%. Possibly

what is required is a solution algorithm that pays more attention to the non-linearities of the flow.

(ii) As a result of complete information not being available on the inlet plane, attempts to satisfy $\nabla \cdot \boldsymbol{q} = 0$ there were not successful. In the event of the "difficult to measure" tangential velocity fields not being specified over the inlet plane for a given flow, a possible solution may, perhaps, be found in the authors observation that when finite-difference numerical calculations are performed on ducted flows where $\nabla \cdot \boldsymbol{q} = 0$ is not solved on the entrance plane, then the tangential velocity field often exhibits discontinuous changes over the first two or three computing planes. Such behaviour probably indicates that the assumed tangential velocity field on the initial plane was a very poor approximation to the actual tangential velocity field, and in changing discontinuously, the tangential velocity fields are trying to assume more realistic patterns. As a consequence it may well be worthwhile trying to develop simple models for tangential velocity fields at entrance planes in order that $\nabla \cdot \boldsymbol{q} = 0$ can be solved at the entrance without forcing an adverse effect upon the flow. A working criteria for such a model could well be the requirement that in the unconstrained flow (i.e. without $\nabla \cdot \boldsymbol{q} = 0$ at inlet) these tangential velocity fields exhibit only smooth changes as they move away from the entrance plane.

It is to be noted that the difference representations $\hat{T}$ used for the momentum operator T (defined by (4)), are not conservative and therefore the schemes do not explicitly conserve energy. However, the diagrams of the constant-total-pressure contours (Figs. 5–7) show that the energy losses were small, particularly in those results obtained with the implementation of the mass-conservation procedure. As a consequence no attempt was made to use the more complicated conservative versions of $\hat{T}$ that may be possibly developed. However, if these conservative versions were to be implemented there would still result a "loss" of energy through the boundaries in exactly the same way that mass was shown to be lost in equation (25). Such a loss could be eliminated by calculating the minor components of velocity $\bar{v}_{i1K}$, $\bar{w}_{i1K}$, $\bar{v}_{iJK}$ and $\bar{w}_{iJK}$ corresponding to the major velocity components $\bar{u}_{i1K}$ and $\bar{u}_{iJK}$ that were used to correct the mass losses through the solid boundaries.

A further, logical, extension of the present procedure would be the use of graded meshes near solid boundaries in order to effectively and economically take account of the sharp velocity gradients near the no-slip /oundaries.

11. Summary of results, and conclusions

All three sets of results use a common difference scheme to represent the velocity terms of the momentum equations.

The method that uses the central-difference formulation for the pressure gradients and continuity terms effectively fails to predict the secondary flow present in the system, despite considerable experimentation with boundary conditions on the pressure equation.

The switch to upwind-downwind schemes for the pressure and continuity terms caused an immediate improvement in the quality of the numerical predictions. It was considered that the quantitative poorness of the results was largely due to numerical losses in mass. A mass-conservation procedure was introduced which resulted in a significant improvement in the quantitative nature of the results, although due to the presence of certain secondary factors the major effect of this procedure was to ensure that mass was lost more or less evenly

throughout the flow, rather than mostly at the solid boundaries. In the authors opinion the success (although limited) of the present method is largely due to two factors. Firstly, the description of the Navier–Stokes equations in the form (8), which enabled one to (a) cope effectively with the geometric terms, and (b) to recognize explicitly that the form of the difference representations of the terms grad p and div $\boldsymbol{q}$ were crucial if the basic form of the continuous operator of the Navier–Stokes equations was to be preserved in its difference representation. The second factor was the deduction that intuitively reasonable *upwind* differencing of pressure gradients implies *downwind* differencing of derivatives in the continuity aquation.

REFERENCES

[1] D. F. Roscoe, The solution of the three-dimensional Navier–Stokes equations using a new finite-difference approach, *Int. J. Num. Meths. Engrg.*, 10 (1976) 1299–1308.

[2] W. Joy, Experimental investigation of shear flow in rectangular bends, *M.Sc. Thesis*, M.I.T., Cambridge, Mass. U.S.A. (1950).

[3] A. R. Stuart and R. Hetherington, The solution of three variable-duct-flow equations, *Proceedings Int. Symp. on Fl. Mech. and Design of Turbo Machinery*, Pittsburgh, (1970).

[4] A. R. Stuart, *Ph. D. Thesis*, University of Aston, (1970).

[5] D. B. Spalding and A. Patankar, A calculation procedure for heat, mass and momentum transfer in three-dimensional parabolic flows, *Int. J. Heat and Mass Transfer* 17 (1972) 1787–1809.

[6] D. F. Roscoe, The application of matrix theorems to the construction of stable difference representations of the equations of fluid dynamics, *Lin. Alg. Applics.*, 14 (1976) 123–130.

[7] F. H. Harlow and J. E. Welch, Numerical calculation of time-dependent viscous incompressible flow of fluid with free surface, *Phys., of Fluids*, 8 (1965) 2182–2189.

[8] W. R. Hawthorne, Secondary circulation in fluid flow, *Proc. Roy. Soc.*, London, 206 (1951) 374–387.

[9] B. Spain, *Tensor calculus*, Oliver and Boyd Ltd., Edinburgh and London, (1965).